# Effects of the $Fe^{3+}$ Spin Transition on the Equation of State of Bridgmanite

Zhu Mao[1,2,3], Jung-Fu Lin[1], Jing Yang[1], Toru Inoue[4], and Vitali B. Prakapenka[5]

[1]Department of Geological Sciences, Jackson School of Geosciences, The University of Texas at Austin, Austin, Texas, USA

[2]Laboratory of Seismology and Physics of Earth's Interior, School of Earth and Planetary Sciences, University of Science and Technology of China, Hefei, Anhui, China

[3]National Geophysics Observatory at Mengcheng, Mengcheng, Anhui, China

[4]Geodynamics Research Center, Ehime University, Matsuyama, Japan

[5]GeoSoilEnviroCARS, University of Chicago, Chicago, IL, USA



This article has been accepted for publication and undergone full peer review but has not been through the copyediting, typesetting, pagination and proofreading process which may lead to differences between this version and the Version of Record. Please cite this article as doi: 10.1002/2015GL064400

**Abstract**

We have investigated the equation of state of Fe-bearing bridgmanite, $(Mg_{0.9}Fe_{0.1})SiO_3$, using synchrotron X-ray diffraction in diamond anvil cells up to 125 GPa and 300 K. Combined with previous synchrotron Mössbauer spectroscopy results, we have found that the occurrence of the low-spin $Fe^{3+}$ in the octahedral sites (B-site) of bridgmanite has produced a 0.5(±0.1)% reduction in the unit cell volume at 18-25 GPa and has increased the isothermal bulk modulus to 284(±4) GPa, consistent with recent theoretical calculations. Together with literature results, we note that the addition of Fe can cause an increase in the density, bulk modulus, and bulk sound velocity in both Al-free and Al-bearing bridgmanite at lower-mantle pressures. The presence of $Fe^{3+}$ in the B-site of bridgmanite can further enhance this increase. The observed spin transition of B-site $Fe^{3+}$ in bridgmanite is thus important for understanding the density states and velocity structure of the lower mantle.

**Key words**: bridgmanite, spin transition, equation of state, lower mantle, density, bulk sound velocity

## 1. Introduction

Earth's lower mantle is believed to mainly consist of bridgmanite [$(Mg,Fe)(Al,Si)O_3$] and ferropericlase [(Mg,Fe)O] with approximately 10% Fe in bridgmanite and 17% Fe in ferropericlase [*Ringwood*, 1975]. Of particular importance is the electronic spin transition of Fe in ferropericlase and bridgmanite which has been reported to affect a number of physical properties, including density, sound velocity, electronic conductivity, etc. [e.g. *Badro et al.*, 2003; *Crowhurst et al.*, 2008; *Goncharov et al.*, 2006; *Lin et al.*, 2013; *Mao et al.*, 2010, 2011a, 2014]. Experimental and theoretical studies on the spin transition of Fe in ferropericlase and bridgmanite thus provide new insights on the physical, chemical, and dynamic states of the lower mantle [e.g. *Badro et al.*, 2004; *Cammarano and Romanowicz*, 2007; *Lin et al.*, 2005; *Wentzcovitch et al.*, 2009].

A review of recent theoretical and experimental results shows that the spin and valence states of iron can affect its stability in different crystallographic sites in bridgmanite [*Lin et al.*, 2013]. For example, $Fe^{2+}$ in bridgmanite is reported to exist in the large dodecahedral sites (A-site) while $Fe^{3+}$ can occupy both the A- and octahedral sites (B-site). Although previous Mö ssbauer spectroscopic studies have shown an abnormal increase in the quadrupole splitting of $Fe^{2+}$ in the A-site of bridgmanite at high pressures, it is still debated whether this change is associated with the high-spin (HS) to intermediate-spin transition of $Fe^{2+}$ in bridgmanite or the change is only a result of the enhanced lattice distortion that does not involve the spin transition [*Hsu et al.*, 2010; *Lin et al.*, 2013; *Lin et al.*, 2012; *McCammon et al.*, 2008]. On the other hand, $Fe^{3+}$ has been reported to occupy both the dodecahedral A-site and the octahedral B-site in bridgmanite. It has been shown that only $Fe^{3+}$ in the B-site

can undergo the HS to low-spin (LS) transition at lower mantle pressures [*Bengtson et al.*, 2009; *Hsu et al.*, 2010; *Lin et al.*, 2013]. It is worth noting that the B-site $Fe^{3+}$ is only reported to be present in the polycrystalline bridgmanite samples, which have been observed to coexist with stishovite (excess silica environment) but is absent in single-crystal bridgmanite [*Ballaran et al.*, 2012; *Catalli et al.*, 2010; *Catalli et al.*, 2011; *Glazyrin et al.*, 2014; *Lin et al.*, 2012; *Potapkin et al.*, 2013]. $Fe^{3+}$ in the B-site of bridgmanite is theoretically predicted to be metastable and only occurs at high pressures and high temperatures [*Hsu et al.*, 2012]. Future investigations are needed to clarify the role of the synthesis conditions (e.g., excess silica, oxygen fugacity) and substitution mechanisms on the presence of B-site $Fe^{3+}$ in bridgmanite.

Recent theoretical studies have shown that the HS to LS transition of $Fe^{3+}$ in bridgmanite occurs at approximately 50 GPa, leading to a volume reduction, softening of the bulk modulus, and causing anomalous variation in the thermal expansion coefficient, heat capacity, and the Grüneisen parameter [*Hsu et al.*, 2011; *Tsuchiya and Wang*, 2013]. Meanwhile, elevating the temperature will broaden the width of the $Fe^{3+}$ spin transition [*Tsuchiya and Wang*, 2013]. The spin transition of $Fe^{3+}$ in bridgmanite has also been identified in experimental studies [*Catalli et al.*, 2010; *Catalli et al.*, 2011; *Lin et al.*, 2012], yet the effect of the $Fe^{3+}$ spin transition on the volume and density of bridgmanite is highly debated and unclear in recent experimental results probably due to the use of inadequate starting samples and pressure medium as well as limited data points. *Catalli et al.* [2011] have shown an anomalous collapse in the volume of an Al-bearing bridgmanite at ~70 GPa where the spin transition of $Fe^{3+}$ occurs, although the Al-bearing bridgmanite is expected to predominantly contain $Fe^{3+}$ in the A-site, which is theoretically predicted to be stable in the

HS state [*Hsu et al.*, 2012].

In this study, we have conducted *in situ* synchrotron X-ray diffraction (XRD) experiments on bridgmanite with 10 mol.% Fe up to 125 GPa and 300 K. Compared to previous studies which did not constrain the spin and valence states of Fe in bridgmanite [*Andrault et al*., 2001; *Ballaran et al.*, 2012; *Dorfman et al.*, 2013], our XRD results obtained from well-characterized bridgmanite samples, together with previous synchrotron Mössbauer spectroscopy (SMS) results, help to better constrain the effects of the Fe spin transition on the equation of state (EoS) of bridgmanite at lower-mantle pressures. Using the obtained results, we have discussed the effect of the Fe spin transition and the variation of Fe and Al content on the density, bulk modulus, and bulk sound velocity of the lower mantle, which aids in understanding the effect of compositional variation on the density and sound velocity of the lower mantle.

**2. Experiments**

Bridgmanite with 10 mol.% Fe (Pv10) was synthesized from enstatite powder, $(Mg_{0.9}Fe_{0.1})SiO_3$, which was synthesized by mixing powders of the oxides MgO, $SiO_2$, and $^{57}Fe_2O_3$ according to the appropriate ratios (see supplementary materials for details) [*Lin et al*., 2012]. The synthesized bridgmanite sample was examined by X-ray diffraction, electron microscope, and Mössbauer spectroscopy (Figure S1) [*Lin et al.*, 2012]. Here, we used the same batch of the bridgmanite sample as *Lin et al.* [2012] which has been examined by the conventional Mö ssbauer spectroscopy at ambient conditions and synchrotron Mö ssbauer spectroscopy measurements (SMS) at high pressures to determine the spin and valence states of Fe. These measurements indicate approximately 20% of the total Fe as $Fe^{3+}$ occupying the

octahedral sites and the remaining 80% as $Fe^{2+}$ in the pseudo-dodecahedral sites.

High-pressure XRD experiments of Pv10 were performed at GSECARS sector of the Advanced Photon Source (APS), Argonne National Laboratory (ANL). The Pv10 samples were polished down to 10-15 μm thick disks which were then loaded into symmetric diamond anvil cells (DACs) with a Re gasket and Ne pressure medium for high-pressure diffraction experiments. Pt powder was placed next to the sample as the pressure calibrant [*Fei et al.*, 2007a]. We have made three runs of XRD measurements, each ranging from 1 bar to 125 GPa (Figure 1 and Table S1). In each run starting at approximately 30 GPa, both the sample and the Pt powder were annealed at ~1500 K by laser heating at every 8-15 GPa pressure step up to 125 GPa in order to reduce the potential deviatoric stress in the sample chamber. Compared to previous studies which synthesized bridgmanite in laser-heated DACs, using well-characterized bridgmanite samples pre-synthesized from a multi-anvil apparatus helped to avoid potential chemical inhomogeneities in the laser-annealed samples [*Andrault et al.*, 2001; *Catalli et al.*, 2010; *Catalli et al.*, 2011; *Dorfman et al.*, 2013; *Mao et al.*, 2011b; *Sinmyo et al.*, 2014]. The diffraction patterns were collected every 2-4 GPa with an X-ray beam of 5×7 μm.

**3. Results**

High-pressure XRD experiments on bridgmanite with 10 mol.% Fe were performed at up to 125 GPa and 300 K using diamond anvil cells (Figures S1 and S2). The obtained XRD patterns of Pv10 match the diffraction lines of bridgmanite (Figure S1). Several weak peaks are identified as diffraction lines of stishovite (Figure S1). About 10-12 diffraction lines were used to calculate the unit cell volume of bridgmanite at each pressure. Comparing the

obtained pressure-volume (*P*-*V*) data of Fe-bearing bridgmanite to that of pure $MgSiO_3$-bridgmanite clearly shows an abnormal reduction of 0.5(±0.1)% in the unit cell volume between 18 and 25 GPa, which has been confirmed by three individual runs of experiments (Figure 1 and Table S1). The abnormal volume reduction is consistent with previous theoretical predictions, which could be associated with the HS to LS transition of $Fe^{3+}$ in the B-site of bridgmanite [*Hsu et al*., 2011; *Tsuchiya et al*., 2013]. Meanwhile, comparing the high-pressure XRD results in this study with previous SMS results that used the same bridgmanite sample indicates that the observed reduction in volume can be mainly associated with the spin transition of the B-site $Fe^{3+}$ in bridgmanite, although the effect of the local site distortion of the A-site $Fe^{2+}$ that concurs with the B-site spin transition remains to be further understood [*Lin et al.*, 2012]. We compare the *P*-*V* relation of Pv10 to pure $MgSiO_3$-bridgmanite, which helps to define the width of the spin transition. The LS fraction of bridgmanite with increasing pressure is calculated as follows (Figure 2) [*Wentzcovitch et al*., 2009]:

$$n_{LS} = \frac{1}{1 + \exp(\Delta G(P,T)^* / T)} \quad (1)$$

where $n_{LS}$ is the LS fraction, $\Delta G(P,T)^*$ is the normalized difference of the Gibbs free energy between the LS and HS state (see supplementary material for details) [*Tsuchiya et al.*, 2006; *Wentzcovitch et al.*, 2009]. These analyses show that the spin transition starts at 18 GPa and completes at 25 GPa (Figure 2). Using the derived width of the spin transition, the *P*-*V* data above 25 GPa fitted to the third-order Birch-Murnahgan EoS yield the isothermal bulk modulus, $K_{T0}$ = 284 (±4) GPa, and unit cell volume, $V_0$ = 162.6 (±0.3) $Å^3$, with a fixed $K_{T0}'$ =

4 for Pv10 with the LS B-site $Fe^{3+}$.

## 4. Discussion and Geophysical Implications

Our high pressure XRD measurements have shown that a sudden collapse in the unit cell volume of Pv10 by 0.5(±0.1)% occurs between 18 and 25 GPa, which corresponds to a 0.6(±0.2)% increase in density. Combining our XRD results with previous SMS results that used the same bridgmanite sample allows us to thoroughly investigate the potential cause for this volume reduction. The high-pressure SMS measurements have shown that the B-site $Fe^{3+}$ undergoes an electronic spin transition at approximately 13-25 GPa while the A-site experiences strong lattice distortions [*Lin et al.*, 2012]. The enhanced volume reduction observed in our XRD measurements is more likely to be associated with the HS to LS transition of $Fe^{3+}$, consistent with previous theoretical studies, although the effect of the increase in the lattice distortion of the A-site $Fe^{2+}$ remains to be further understood [*Hsu et al.*, 2011; *Tsuchiya et al.*, 2013]. Moreover, our results support recently predicted theoretical results in which bridgmanite having 6.25-12.5% $Fe^{3+}/(Fe^{2+}+Fe^{3+})$ in the B site undergoes across the $Fe^{3+}$ spin transition with a 0.7-1.2% volume reduction at 40-50 GPa (Figure 2) [*Hsu et al.*, 2011; *Tsuchiya and Wang*, 2013]. Although two experimental studies have also documented the spin transition of $Fe^{3+}$ in bridgmanite, the effect of the potential $Fe^{3+}$ spin transition on the EoS of bridgmanite cannot be quantitatively evaluated because of the limited data points and the stiffer pressure medium used (Figure 2) [*Catalli et al.*, 2010; *Catalli et al.*, 2011]. It should be noted that all of the samples used in this study were well characterized and were loaded with Ne, a softer pressure medium as compared to the previous experimental studies [*Catalli et al.*, 2010; *Catalli et al.*, 2011]. In order to better understand the effects of

the B-site $Fe^{3+}$ spin transition on the EoS parameters of Fe-bearing bridgmanite, we have used bridgmanite samples which were pre-synthesized from enstatite powder using the large-volume press. The spin and valence states of Fe as well as chemical homogeneity of the bridgmanite sample have been characterized using Mö ssbauer spectroscopy, X-ray diffraction and electron microprobe analyses at ambient conditions, while synchrotron Mö ssbauer spectroscopy results of the sample at high pressures have revealed the B-site $Fe^{3+}$ spin transition at approximately 13-24 GPa that can be directly combined with our EoS data. We should note that although there have been a number of previous in situ studies on the spin and valence states of iron and their effects on the EoS of bridgmanite, some of these previous studies had used bridgmanite samples synthesized using laser heating from polycrystalline enstatite or glass starting samples [*Catalli et al.*, 2010; *Catalli et al.*, 2011], which could develop rather complex chemistry and iron valence states due to laser heating conditions.

The onset pressure of the spin transition could be much lower than that in literature reports because of much lower $Fe^{3+}$ content in our bridgmanite (Figure 2) [*Catalli et al.*, 2010; *Catalli et al.*, 2011; *Hsu et al.*, 2011; *Tsuchiya and Wang*, 2013]. Although *Bengtson et al.* [2008] predicted that the spin transition pressure of $Fe^{3+}$ in bridgmanite is independent of the Fe content up to 25%, previous XRD and SMS measurements have shown that the onset pressure of the $Fe^{2+}$ spin transition for ferropericlase and the $Fe^{3+}$ spin transition for bridgmanite increases with the Fe content [*Catalli et al.*, 2010; *Catalli et al.*, 2011; *Fei et al.*, 2007b; *Jackson et al.*, 2005; *Lin et al.*, 2012]. The onset pressure of the spin transition could be much lower than that in literature reports because of much lower $Fe^{3+}$ content in our bridgmanite [*Catalli et al.*, 2010; *Catalli et al.*, 2011; *Hsu et al.*, 2011; *Tsuchiya and Wang*,

2013]. It is also worth noting that $Fe^{3+}$ enters the lower-mantle bridgmanite either by the coupled-substitution of $Mg^{2+}$ and $Si^{4+}$ by $Al^{3+}$ and $Fe^{3+}$ or the self-disproportionation of $Fe^{2+}$ to $Fe^{3+}$ plus metallic iron [*Frost et al.*, 2004; *Hummer and Fei*, 2012; *Zhang and Oganov*, 2006]. Although the lower-mantle $Fe^{3+}$ in bridgmanite could be as high as 60% [$Fe^{3+}/(Fe^{3+}+Fe^{2+})$], most of the $Fe^{3+}$ will be located in the A-site, while only a small amount of $Fe^{3+}$ could be in the B-site [*Ballaran et al.*, 2012; *Frost et al.*, 2004; *Hummer and Fei*, 2012; *McCammon*, 1997]. This will be particularly true when the dissolution of Al-bearing majorite into Al-bearing bridgmanite occurs at pressures of 25-30 GPa of the top lower mantle [*Irifune et al.*, 2010]. A previous study has shown that the amount of Al will increase in bridgmanite with the pressure of the top lower mantle together with an increase in the Fe content with the coupled-substitution [*Irifune et al.*, 2010]. Since Al will be located in the B-site of bridgmanite, the addition of $Fe^{3+}$ in bridgmanite at the top lower mantle will be mainly located in the A-site. $Fe^{3+}$ in the B-site of bridgmanite is thus significantly limited by the addition of Al in bridgmanite. Since the amount of B-site $Fe^{3+}$ in the lower-mantle bridgmanite is low, the onset pressure of the $Fe^{3+}$ spin transition could also be low in the lower mantle, similar to that shown in our study [*Catalli et al.*, 2010; *Catalli et al.*, 2011; *Hsu et al.*, 2011; *Tsuchiya and Wang*, 2013].

We have noted that the spin transition of $Fe^{3+}$ in the B-site of bridgmanite has only been reported in a few high-pressure studies which used powder bridgmanite samples synthesized at high pressures using $Fe^{3+}$-bearing or Fe-rich material as the starting sample in laser-heated DACs for XRD and/or SMS experiments, in which the SMS results play a critical role in identifying the LS $Fe^{3+}$ in the synthesized bridgmanite [*Catalli et al.*, 2010; *Catalli et al.*,

2011; *Mao et al.*, 2011b]. In single-crystal studies, $Fe^{3+}$ tends to be located in the large A-site in bridgmanite [*Ballaran et al.*, 2012; *Glazyrin et al.*, 2014; *Potapkin et al.*, 2013]. It is possible that the substitution of $Fe^{3+}$ in the octahedral sites in bridgmanite powder samples is related to the starting material, synthesis conditions, and/or pressure-temperature environments of the experiments. Even with a $Fe^{2+}$-bearing starting material, polycrystalline bridgmanite synthesized at large volume pressure which is in a more $O_2$ open environment may be more likely to have LS $Fe^{3+}$ than that synthesized in DACs [*Andrault et al.*, 2001; *Lundin et al.*, 2008]. On the other hand, the use of the $Fe^{3+}$-containing starting material may also promote the presence of LS B-site $Fe^{3+}$ [*Catalli et al.*, 2010; *Catalli et al.*, 2011]. *Mao et al.*, [2011b] reported the observation of LS B-site $Fe^{3+}$ in the Fe-enriched bridgmanite. Although *Dorfman et al.*, [2013] studied two Fe-rich bridgmanite, the spin and valence states of Fe in their synthesized bridgamnite samples were unknown. The pressure-temperature-dependent substitution mechanism of Fe in the bridgmanite's lattice, such as the charge-coupled substitution, vacancies, and/or charge transfer, together with the starting material on the spin states of Fe in bridgmanite remain to be further investigated in future studies.

We have further examined the effect of Fe content on the density ($\rho_0$) and bulk modulus ($K_0$) of bridgmanite at ambient conditions (Figures 3 and S4, Table S2) [*Andrault et al.*, 2001; *Ballaran et al.*, 2012; *Catalli et al.*, 2010; *Catalli et al.*, 2011; *Dorfman et al.*, 2013; *Lundin et al.*, 2008; *Mao et al.*, 2011b]. Although *Dorfman et al.*, [2013] reported the EoS of bridgmanite with up to 74% Fe, we focus on the Fe-dilute systems in Figure 3 because of the coexistence of bridgmanite with other Fe-bearing phases in *Dorfman et al.*, [2013], which

could lead to the depletion of Fe in their synthesized bridgmanite. Here the Fe content defined as Fe/(Fe+Mg) refers to the total molar percentage of Fe. It is worth noting that a long-standing problem in comparing the equation of state parameters of mantle minerals to literature results is that different studies use different pressure calibrants and scales. Although most previous studies for the EoS of bridgmanite used Au as the pressure calibrant, which is different from the Pt calibrant used here, we have re-calculated the pressure in literature using the Au pressure scale in *Fei et al*., [2007a], which reported an internally consistent pressure scale for Pt and Au (Table S2) [*Andrault et al.*, 2001; *Ballaran et al.*, 2012; *Catalli et al.*, 2010; *Catalli et al.*, 2011; *Dorfman et al.*, 2013; *Lundin et al.*, 2008; *Mao et al.*, 2011b]. In addition, *Andrault et al*., [2001] and *Ballaran et al*., [2012] used Ruby as the pressure calibrant. Pressures in these two studies are re-calibrated using the pressure scales from *Dewaele et al.* [2004], which is in a good agreement with the metal pressure scales in *Fei et al*., [2007a]. Relevant literature *P*-*V* data were re-analyzed using a third-order Birch-Murnaghan EoS with a fixed $K_0$'=4 in order to have a more consistent, direct comparison of $\rho_0$ and $K_0$ from different studies (Table S2 and Figure 3). $\rho_0$ is directly measured by XRD in most previous studies although these studies did not report the spin transition of $Fe^{3+}$ in bridgmanite [*Andrault et al.*, 2001; *Ballaran et al.*, 2012; *Lundin et al.*, 2008]. For bridgmanite with the LS B-site $Fe^{3+}$, $\rho_0$ is derived by fitting the experimental *P*-*V* data using the third-order Birch-Murnaghan EoS, which suffers from a well-known trade-off between the derived $K_0$ and $K_0$' values [*Catalli et al.*, 2010; *Catalli et al.*, 2011; *Mao et al.*, 2011b]. The confidence ellipses are constructed for bridgmanite with the LS B-site $Fe^{3+}$ to better understand the trade-off between the derived $\rho_0$ ($V_0$) and $K_0$ values (Figure S5).

For Al-free bridgmanite without abnormal changes in the *P-V* data, $\rho_0$ linearly increases with the Fe content, while $K_0$ is independent of the Fe content when taking the uncertainties into consideration (Figure 3). The spin transition of the B-site $Fe^{3+}$ in bridgmanite is found to enhance $\rho_0$ and $K_0$ to above the linear relation. The increase in $\rho_0$ of our Pv10 is less than that in *Catalli et al.* [2010] and*Mao et al.* [2011b], which could be due to a lower LS $Fe^{3+}$ content in our Pv10. $\rho_0$ and $K_0$ of Al-bearing bridgmanite are not nearly as well constrained as those in the Al-free counterparts because of limited experimental studies available [*Andrault et al.*, 2001; *Ballaran et al.*, 2012; *Catalli et al.*, 2011; *Glazyrin et al.*, 2014]. In the Al-dilute system, the density of Al-bearing bridgmanite is slightly lower than that of Al-free bridgmanite with the same Fe content [*Andrault et al.*, 2001]. The relationship between $K_0$ and the Fe content is difficult to be evaluated quantitatively because only *Andrault et al.* [2001] studied the EoS of bridgmanite in the Al-dilute system. It is interesting to note that *Glazyrin et al.* [2014] studied the EoS of $Fe^{3+}$- and $Al^{3+}$-enriched bridgmanite at lower-mantle pressure and temperature conditions. Addition of $Fe^{3+}$ in the A-site together with the presence of $Al^{3+}$ in the B-site can result in a great reduction in $K_0$, indicating the importance of exploring the effect of oxidation state on the EoS of lower-mantle bridgmanite in future studies [*Glazyrin et al.*, 2014]. In contrast, the spin transition of the B-site $Fe^{3+}$ can cause an increase in both $\rho_0$ and $K_0$ in Al-bearing bridgmanite, which is similar to that shown in Al-free bridgmanite [*Catalli et al.*, 2011].

We have modeled the variation of $\rho$, $K$, and bulk sound velocity ($V_\Phi$) of bridgmanite at lower-mantle pressures and 300 K using $MgSiO_3$ bridgmanite as the reference (Figure 4) (see supplementary material for details). For Al-free bridgmanite without abnormal changes in the

*P-V* data, the difference in density between Al-free and $MgSiO_3$ bridgmanite is almost constant with pressure because $K_0$ is independent of Fe content (Figure 4). Since the spin transition of the B-site $Fe^{3+}$ increases the stiffness of bridgmanite, the difference in density between bridgmanite with the LS $Fe^{3+}$ and $MgSiO_3$ endmember exhibits a decrease with increasing pressure. At pressures corresponding to the lowermost mantle, $\rho$ of our Pv10 with the LS $Fe^{3+}$ is undistinguishable from that of Pv4 within uncertainties of the EoS modeling [*Ballaran et al.*, 2012]. Furthermore, raising the amount of the LS $Fe^{3+}$ in bridgmanite may increase the density difference between the Fe-bearing and $MgSiO_3$ endmembers (Figure 4) [*Catalli et al.*, 2010]. On the other hand, $K$ and $V_\Phi$ of our Pv10 with the LS $Fe^{3+}$ in the B-site are 6-9(±3)% and 2-3.5(±1.5)% greater than those of $MgSiO_3$ bridgmanite at lower-mantle pressures, respectively (Figure 4). These values are also much greater than that of Al-free bridgmanite in literature which does not clearly exhibit an abnormal change in the unit cell volume at high pressures. To better understand the effect of Fe and Al on the EoS of bridgmanite, we also compute the variation of $\rho$, $K$, and $V_\Phi$ of $(Mg_{0.9}Fe_{0.1})(Al_{0.1}Si_{0.9})O_3$ bridgmanite. In the analyses, we assumed that all of the Fe was in the HS state, the same $K_0$ as the $MgSiO_3$ end-member, and used the linear relation in Figure 3 to derive the density. Comparing the variation of $\rho$, $K$, and $V_\Phi$ of $(Mg_{0.9}Fe_{0.1})(Al_{0.1}Si_{0.9})O_3$-bridgmanite without the LS $Fe^{3+}$ to results in *Catalli et al.* [2011] provides a first-order estimation on the effect of LS $Fe^{3+}$ in Al-bearing bridgmanite. It is shown that Al-bearing bridgmanite with the LS $Fe^{3+}$ in the B-site also has a greater $\rho$, $K$, and $V_\Phi$ at lower mantle pressures than bridgmanite without the LS $Fe^{3+}$ at lower mantle pressures (Figure 4). Since the EoS of the Al-bearing bridgmanite is not as well constrained as the Fe-bearing ones, more reliable data are needed in the future

to provide a better understanding of the combined effects of Fe spin state as well as Fe and Al content on the density profiles and velocity structures of the lower mantle.

Our study here has shown that the spin transition of $Fe^{3+}$ can cause a sudden reduction in the volume and an increase in the bulk modulus of lower-mantle bridgmanite, which is consistent with recent theoretical predictions. Using a well-characterized bridgmanite sample by combining XRD, conventional Mö ssbauer spectroscopy, and SMS allows us to better constrain the spin and valence states of Fe in bridgmanite and understand the effect of spin transition on the density and bulk modulus bridgmanite. Based on our current understanding of the phase diagram of the (Al,Fe)-bearing $MgSiO_3$-$Mg_2SiO_4$ system at mantle P-T conditions, bridgmanite starts to contain more significant amount of Al at pressures above approximately 28 GPa where majoritic garnet, the major host of Al in the transition zone and very top of the lower mantle, becomes unstable and forms solid solution with bridgmanite [*Irifune et al.*, 2010]. Therefore, it is possible that the B-site $Fe^{3+}$ can exist in the bridgmanite's lattice at conditions of the topmost lower-mantle, but would become much less abundant at higher pressures when Al extensively dissolves into the bridgmanite. The effects of the spin transition of B-site $Fe^{3+}$ in bridgmanite observed here are thus most applicable to understand the properties of the topmost lower mantle, where the spin transition can lead to enhanced density and elevated bulk sound velocity in bridgmanite than previously thought for a high-spin bridgmanite. However, if the amount of B-site $Fe^{3+}$ in the lower-mantle bridgmanite is less than that in our bridgmanite sample containing 20% B-site $Fe^{3+}$, the effect of $Fe^{3+}$ spin transition on the density and bulk sound velocity of bridgmanite could be greatly reduced or even become negligible geophysically. Future studies are expected to explore how

the $Fe^{3+}$ content and temperature affects the onset pressure of the spin transition and the thermoelastic properties of bridgmanite, which is of particular importance for understanding the density states, velocity structure, and dynamic behaviors of the lower mantle.

**Acknowledgements**

We acknowledge J. Liu for experimental assistance and M. Matheney, I. A. Kuang, and L. Dafov for editing the manuscript. We thank GSECARS, HPCAT, APS, and ANL for providing X-ray diffraction facilities for the study. Z.M. acknowledges financial support from the National Natural Science Foundation of China (41374092) and the Fundamental Research Funds for the Central Universities in China (WK2080000052). J.F.L. acknowledges financial support from the US National Science Foundation (EAR-0838221 and EAR-1053446) and the Carnegie/DOE Alliance Center (CDAC). APS is supported by DOE-BES, under Contract No. DE-AC02-06CH11357. GeoSoilEnviroCARS is supported by the National Science Foundation - Earth Sciences **(**EAR-1128799) and Department of Energy Geosciences (DE-FG02-94ER14466). Experimental data and parameters for modeling Figure 3 and 4 are available in the Supplementary Materials.

**References**

Andrault, D., N. Bolfan-Casanova, and N. Guignot (2001), Equation of state of lower mantle (Al,Fe)-$MgSiO_3$ perovskite, *Earth Planet Sci. Lett.*, *193*, 501-508.

Badro, J., J. P. Rueff, G. Vanko, G. Monaco, G. Fiquet, and F. Guyot (2004), Electronic transitions in perovskite: Possible nonconvecting layers in the lower mantle, *Science*, *305*, 383-386.

Badro, J., G. Fiquet, F. Guyot, J. P. Rueff, V. V. Struzhkin, G. Vanko, and G. Monaco (2003), Iron partitioning in Earth's mantle: Toward a deep lower mantle discontinuity, *Science*, *300*, 789-791.

Ballaran, T. B., A. Kurnosov, K. Glazyrin, D. J. Frost, M. Merlini, M. Hanfland, and R. Caracas (2012), Effect of chemistry on the compressibility of silicate perovskite in the lower mantle, *Earth Planet Sci. Lett.*, *333*, 181-190.

Bengtson, A., K. Persson, and D. Morgan (2008), *Ab initio* study of the composition

dependence of the pressure-induced spin crossover in perovskite (Mg1-xFex)SiO3, *Earth Planet Sci. Lett., 265*, 535-545.
Bengtson, A., J. Li, and D. Morgan (2009), Mössbauer modeling to interpret the spin state of iron in (Mg,Fe)SiO3 perovskite, *Geophys. Res. Lett., 36*, doi: 10.1029/2009GL038340.
Cammarano, F., and B. Romanowicz (2007), Insights into the nature of the transition zone from physically constrained inversion of long-period seismic data, *P. Natl. Acad. Sci. USA., 104*, 9139-9144.
Catalli, K., S. H. Shim, V. B. Prakapenka, J. Y. Zhao, W. Sturhahn, P. Chow, Y. M. Xiao, H. Z. Liu, H. Cynn, and W. J. Evans (2010), Spin state of ferric iron in $MgSiO_3$ perovskite and its effect on elastic properties, *Earth Planet Sci. Lett., 289*, 68-75.
Catalli, K., S. H. Shim, P. Dera, V. B. Prakapenka, J. Y. Zhao, W. Sturhahn, P. Chow, Y. M. Xiao, H. Cynn, and W. J. Evans (2011), Effects of the $Fe^{3+}$ spin transition on the properties of aluminous perovskite-New insights for lower-mantle seismic heterogeneities, *Earth Planet Sci. Lett., 310*, 293-302.
Crowhurst, J. C., J. M. Brown, A. F. Goncharov, and S. D. Jacobsen (2008), Elasticity of (Mg,Fe)O through the spin transition of iron in the lower mantle, *Science, 319*, 451-453.
Dewaele, A., P. Loubeyre, and M. Mezouar (2004), Equations of state of six metals above 94 GPa, *Phys. Rev. B., 70*, 094112.
Dorfman, S., Y. Meng, V. Prakapenka, and T. S. Duffy (2013), Effect of Fe-enrichment on the equation of state and stability of $(Mg,Fe)SiO_3$ perovskite, *Earth Planet Sci. Lett., 361*, 246-257.
Fei, Y. W., A. Ricolleau, M. Frank, K. Mibe, G. Y. Shen, and V. Prakapenka (2007a), Toward an internally consistent pressure scale, *P. Natl. Acad. Sci. USA., 104*, 9182-9186.
Fei, Y. W., L. Zhang, A. Corgne, H. Watson, A. Ricolleau, Y. Meng, and V. Prakapenka (2007b), Spin transition and equations of state of (Mg, Fe)O solid solutions, *Geophys. Res. Lett., 34*, doi: 10.1029/2007GL030712.
Fiquet, G., A. Dewaele, D. Andrault, M. Kunz, and T. Le Bihan (2000), Thermoelastic properties and crystal structure of $MgSiO_3$ perovskite at lower mantle pressure and temperature conditions, *Geophys. Res. Lett., 27*, 21-24.
Frost, D. J., C. Liebske, F. Langenhorst, C. A. McCammon, R. G. Tronnes, and D. C. Rubie (2004), Experimental evidence for the existence of iron-rich metal in the Earth's lower mantle, *Nature, 428*, 409-412.
Glazyrin, K., T. B. Ballaran, D. J. Frost, C. McCammon, A. Kantor, M. Merlini, M. Hanfland, and L. Dubrovinsky (2014), Magnesium silicate perovskite and effect of iron oxidation state on its bulk sound velocity at the conditions of the lower mantle, *Earth Planet Sci. Lett., 393*, 182-186.
Goncharov, A. F., V. V. Struzhkin, and S. D. Jacobsen (2006), Reduced radiative conductivity of low-spin (Mg,Fe)O in the lower mantle, *Science, 312*, 1205-1208.
Hsu, H., Y. G. Yu, and R. M. Wentzcovitch (2012), Spin crossover of iron in aluminous $MgSiO_3$ perovskite and post-perovskite, *Earth Planet Sci. Lett., 359-360*, 34-39.
Hsu, H., K. Umemoto, P. Blaha, and R. M. Wentzcovitch (2010), Spin states and hyperfine interactions of iron in $(Mg,Fe)SiO_3$ perovskite under pressure, *Earth Planet Sci. Lett., 294*, 19-26.
Hsu, H., P. Blaha, M. Cococcioni, and R. M. Wentzcovitch (2011), Spin-state crossover and

hyperfine interactions of ferric iron in $MgSiO_3$ perovskite, *Phys.Rev.Lett.*, *106*, 118501.
Hummer, D. R., and Y. W. Fei (2012), Synthesis and crystal chemistry of $Fe^{3+}$-bearing $(Mg,Fe^{3+})(Si,Fe^{3+})O_3$ perovskite, *Am. Mineral.*, *97*, 1915-1921.
Irifune, T., T. Shinmei, C. A. McCammon, N. Miyajima, D. C. Rubie, and D. J. Frost (2010), Iron partitioning and density changes of pyrolite in Earth's lower mantle, *Science*, *327*, 193-195.
Jackson, J. M., W. Sturhahn, G. Y. Shen, J. Y. Zhao, M. Y. Hu, D. Errandonea, J. D. Bass, and Y. W. Fei (2005), A synchrotron Mössbauer spectroscopy study of $(Mg,Fe)SiO_3$ perovskite up to 120 GPa, *Am. Mineral.*, *90*, 199-205.
Lin, J. F., S. Speziale, Z. Mao, and H. Marquardt (2013), Effects of the electronic spin transitions of iron in lower-mantle minerals: implications to deep-mantle geophysics and geochemistry, *Rev. Geophys.*, *51*, 2012RG000414.
Lin, J. F., E. E. Alp, Z. Mao, T. Inoue, C. McCammon, Y. M. Xia, P. Chow, and J. Y. Zhao (2012), Electronic spin states of ferric and ferrous iron in the lower-mantle silicate perovskite, *Am. Mineral.*, *97*, 592-597.
Lin, J. F., V. V. Struzhkin, S. D. Jacobsen, M. Y. Hu, P. Chow, J. Kung, H. Z. Liu, H. K. Mao, and R. J. Hemley (2005), Spin transition of iron in magnesiowustite in the Earth's lower mantle, *Nature*, *436*, 377-380.
Lundin, S., K. Catalli, J. Santillan, S. H. Shim, V. B. Prakapenka, M. Kunz, and Y. Meng (2008), Effect of Fe on the equation of state of mantle silicate perovskite over 1 Mbar, *Phys. Earth Planet Int.*, *168*(1-2), 97-102.
Mao, Z., J. F. Lin, C. Jacobs, H. C. Watson, Y. Xiao, P. Chow, E. E. Alp, and V. B. Prakapenka (2010), Electronic spin and valence states of Fe in $CaIrO_3$-type silicate post-perovskite in the Earth's lowermost mantle, *Geophys. Res. Lett.*, *37*, doi: 10.1029/2010GL045021.
Mao, Z., J. F. Lin, J. Liu, and V. B. Prakapenka (2011a), Thermal equation of state of lower-mantle ferropericlase across the spin crossover, *Geophys. Res. Lett.*, *38*, doi: 10.1029/2011GL049915.
Mao, Z., J. F. Lin, H. P. Scott, H. C. Watson, V. B. Prakapenka, Y. Xiao, P. Chow, and C. McCammon (2011b), Iron-rich perovskite in the Earth's lower mantle, *Earth Planet Sci. Lett.*, *309*, 179-184.
Mao, Z., J. F. Lin, J. Yang, H. Bian, J. Liu, H. C. Watson, S. Huang, J. H. Chen, V. B. Prakapenka, Y. M. Xiao, and P. Chow (2014b), (Fe, Al)-bearing post-perovskite in the Earth's lower mantle, *Earth Planet Sci. Lett.*, *403*, 157-165.
McCammon, C. (1997), Perovskite as a possible sink for ferric iron in the lower mantle, *Nature*, *387*, 694-696.
McCammon, C., I. Kantor, O. Narygina, J. Rouquette, U. Ponkratz, I. Sergueev, M. Mezouar, V. Prakapenka, and L. Dubrovinsky (2008), Stable intermediate-spin ferrous iron in lower-mantle perovskite, *Nat. Geosci.*, *1*, 684-687.
Potapkin, V., et al. (2013), Effect of iron oxidation state on the electrical conductivity of the Earth's lower mantle, *Nature Communications*, *4*, doi:10.1038/ncomms2436.
Ringwood, A. E. (1975), *Composition and petrology of the Earth's mantle*, 618 pp., McGraw-Hill, New York.
Sinmyo, R., G. Pesce, E. Greenberg, C. McCammon, and L. Dubrovinsky (2014), Lower

mantle electrical conductivity based on measurements of Al, Fe-bearing perovskite under lower mantle conditions, *Earth Planet Sci. Lett.*, *393*, 165-172.

Tsuchiya, T., and X. Wang (2013), Ab initio investigation on the high-temperature thermodynamic properties of $Fe^{3+}$-bearing $MgSiO_3$ perovskite, *J. Geophys. Res.*, *118*, 83-91.

Tsuchiya, T., R. M. Wentzcovitch, C. R. S. da Silva, and S. de Gironcoli (2006), Spin transition in magnesiowustite in earth's lower mantle, *Phys.Rev.Lett.*, *96*, 198501.

Wentzcovitch, R. M., J. F. Justo, Z. Wu, C. R. S. da Silva, D. A. Yuen, and D. Kohlstedt (2009), Anomalous compressibility of ferropericlase throughout the iron spin cross-over, *P. Natl. Acad. Sci. USA.*, *106*(21), 8447-8452.

Zhang, F. W., and A. R. Oganov (2006), Mechanisms of $Al^{3+}$ incorporation in $MgSiO_3$ post-perovskite at high pressures, *Earth Planet Sci. Lett.*, *248*(1-2), 69-76.

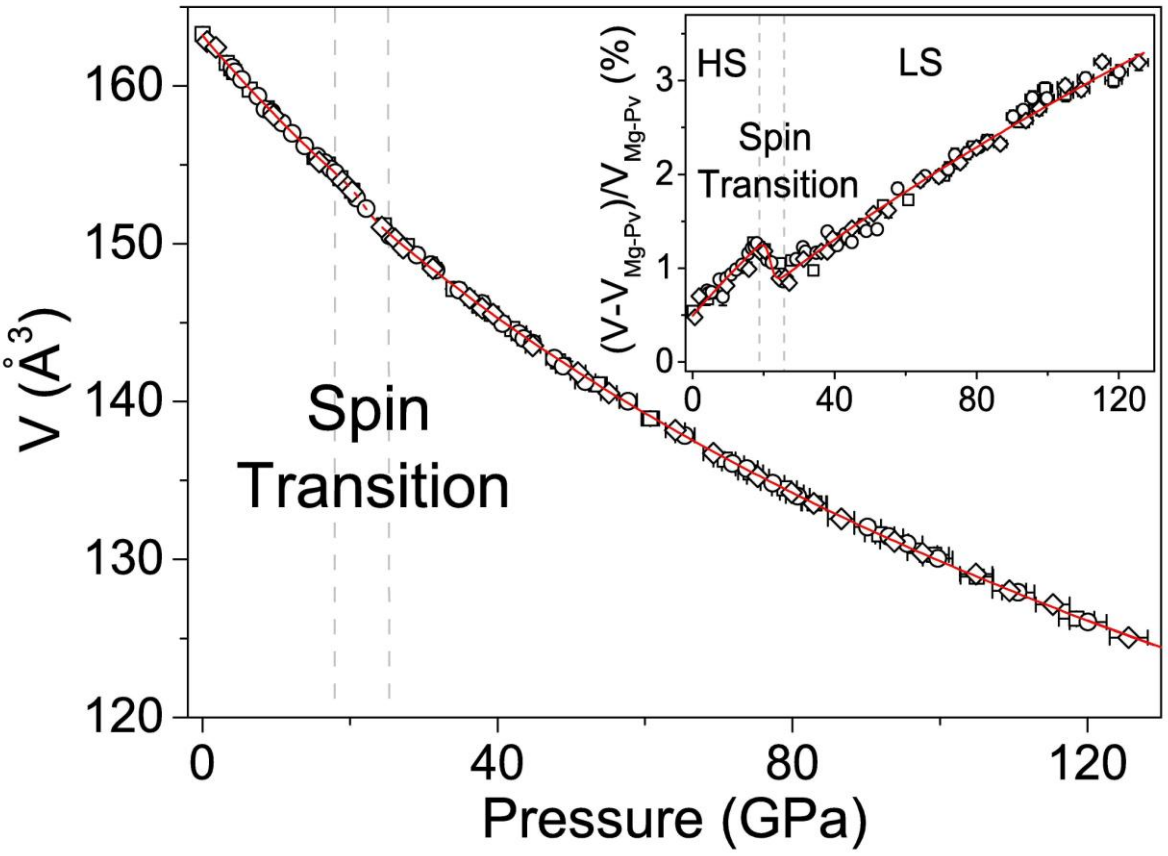


Figure 1. Pressure-volume relations of silicate bridgmanite. Square, circle and diamonds: experimental data for the 1st, 2nd, and 3rd run, respectively; red lines: EoS of bridgmanite; red dashed lines: bridgmanite with mixed HS and LS $Fe^{3+}$. The vertical grey dashed lines indicate the region with mixed HS and LS $Fe^{3+}$. The insert figure shows the variation of the unit cell volume of bridgmanite with pressure using end-member $MgSiO_3$ bridgmanite as the reference, $(V-V_{Mg\text{-}Pv})/ V_{Mg\text{-}Pv}$ [*Ballaran et al.*, 2012]. Errors are smaller than symbols when not shown.

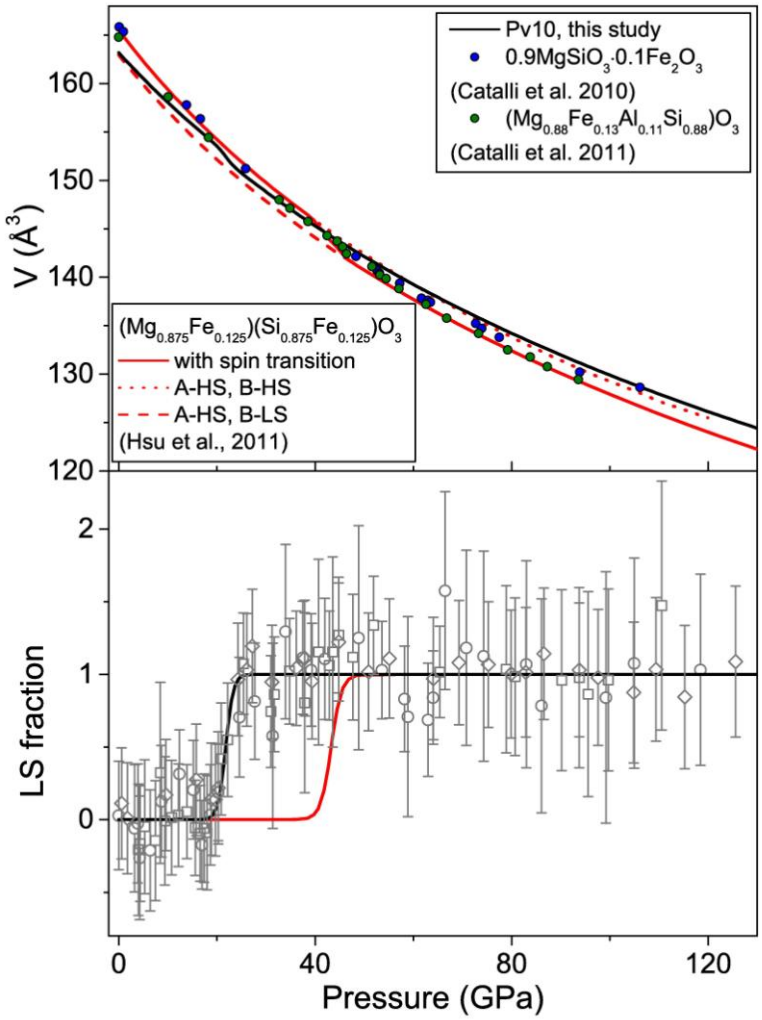


Figure 2. Pressure-volume relations (a) and low-spin fraction (b) of silicate bridgmanite (Pv10) compared with previous experimental and theoretical calculations. (a). Black line: Pv10, this study; red lines: $(Mg_{0.875},Fe_{0.125})(Si_{0.875},Fe_{0.125})O_3$-bridgmanite [*Hsu et al.*, 2011]; green and blue circles: experimental results [*Catalli et al.*, 2010; *Catalli et al.*, 2011]; (b). Open square, circle, and diamonds: experimental LS fraction of $Fe^{3+}$ in bridgmanite in the 1st, 2nd, and 3rd run, respectively (this study); black lines: fitting results for the LS fraction of $Fe^{3+}$ in bridgmanite (this study); red line: theoretically-calculated LS fraction of $Fe^{3+}$ in Pv25 [*Hsu et al.*, 2011].

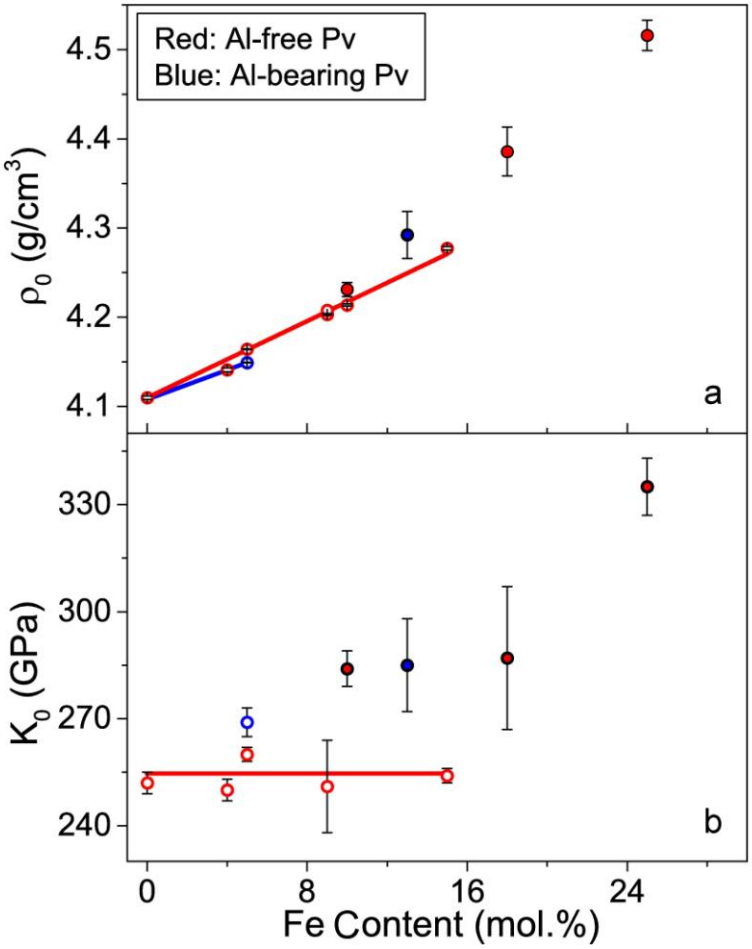


Figure 3. Density, $\rho_0$, (a) and bulk modulus, $K_0$, (b) of bridgmanite at ambient conditions. Red open circles and line: Al-free bridgmanite in literature without an apparent abnormal change in the *P-V* data [*Ballaran et al.*, 2012; *Dorfman et al.*, 2013; *Fiquet et al.*, 2000; *Lundin et al.*, 2008]; red solid circles: Al-free bridgmanite with LS $Fe^{3+}$ [This study; *Catalli et al.*, 2010; *Mao et al.*, 2011b]; blue open circles and line: Al-bearing bridgmanite without an apparent abnormal change in the *P-V* data [*Andrault et al.*, 2001]; blue solid circles: Al-bearing bridgmanite with LS $Fe^{3+}$ [*Catalli et al.*, 2011]. Results for bridgmanite with LS $Fe^{3+}$ are derived using experimental data at pressures above the spin transition [This study; *Catalli et al.*, 2010; *Catalli et al.*, 2011; *Mao et al.*, 2011b]. Errors are smaller than symbols when not shown.

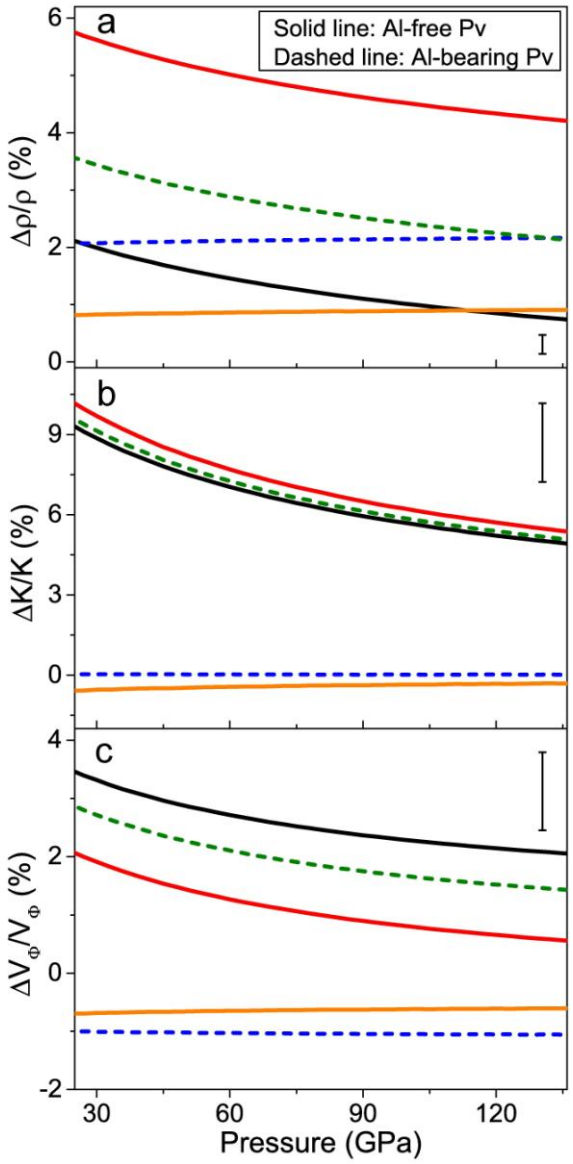


Figure 4. Variation of density (a), bulk modulus (b), and bulk sound velocity (c) of bridgmanite at lower-mantle pressures using $MgSiO_3$ bridgmanite as the reference. Solid lines: Al-free bridgmanite; dashed lines: Al-bearing bridgmanite; orange line: Al-free bridgmanite with 4 mol.% Fe [*Ballaran et al.*, 2012]; black line: Al-free bridgmanite with the LS $Fe^{3+}$ (Pv10), this study; red line: Al-free bridgmanite with the LS $Fe^{3+}$ [*Catalli et al.*, 2010]; blue dashed line: $(Mg_{0.9}Fe_{0.1})(Al_{0.1}Si_{0.9})O_3$-bridgmanite without the LS $Fe^{3+}$; green dashed line: Al-bearing bridgmanite with the LS $Fe^{3+}$ [*Catalli et al.*, 2011].